

Helmholtz Decomposition and Boundary Element Method Applied to Dynamic Linear Elastic Problems

Evert Klaseboer¹  · Qiang Sun²  ·
Derek Y.C. Chan^{3,4} 

Received: 5 June 2018 / Published online: 11 December 2018
© Springer Nature B.V. 2018

Abstract The displacement field for three dimensional dynamic elasticity problems in the frequency domain can be decomposed into a sum of a longitudinal and a transversal part known as a Helmholtz decomposition. The Cartesian components of both the longitudinal and transverse fields satisfy scalar Helmholtz equations that can be solved using a desingularized boundary element method (BEM) framework. The curl free longitudinal and divergence free transversal conditions can also be cast as additional scalar Helmholtz equations. When compared to other BEM implementations, the current framework leads to smaller matrix dimensions and a simpler conceptual approach. The numerical implementation of this approach is benchmarked against the 3D elastic wave field generated by a rigid vibrating sphere embedded in an infinite linear elastic medium for which the analytical solution has been derived. Examples of focused 3D elastic waves generated by a vibrating bowl-shaped rigid object with convex and concave surfaces are also considered. In the static zero frequency limit, the Helmholtz decomposition becomes non-unique, and both the longitidi-

This work is supported in part by the Australian Research Council through a Discovery Early Career Researcher Award DE150100169 to QS and a Discovery Project Grant DP170100376 to DYCC.

Electronic supplementary material The online version of this article (<https://doi.org/10.1007/s10659-018-09710-y>) contains supplementary material, which is available to authorized users.

✉ Q. Sun
Qiang.Sun@unimelb.edu.au
E. Klaseboer
evert@ihpc.a-star.edu.sg
D.Y.C. Chan
D.Chan@unimelb.edu.au

¹ Institute of High Performance Computing, 1 Fusionopolis Way, Singapore 138632, Singapore

² Particulate Fluids Processing Center, Department of Chemical Engineering, The University of Melbourne, Parkville 3010, VIC, Australia

³ School of Mathematics and Statistics, The University of Melbourne, Parkville 3010, VIC, Australia

⁴ Department of Mathematics, Swinburne University of Technology, Hawthorn 3122, VIC, Australia

nal and transverse components contain divergent terms that are proportional to the inverse square of the frequency. However, these divergences are equal and opposite so that their sum, that is the displacement field that reflects the physics of the problem, remains finite in the zero frequency limit.

Keywords Harmonic waves in the frequency domain · Desingularized boundary element method · Navier equation · Helmholtz equation

Mathematics Subject Classification (2010) 74B05 · 35J05 · 35Q74 · 65M38

1 Introduction

Numerical modeling using dynamic linear elasticity theory has found applications in many fields. It has been used in areas such as geological surveys, earth-soil interaction, sound reduction, crack detection [1] or even in earthquake propagation studies [2]. Currently, there is renewed interest in this area due to advances in the development of ultrasonic and microfluidic based devices for trapping of biological cells and micro particles [3].

An extensive review of early analytic treatments of the theory of dynamic elasticity is given by Sternberg [4] who, according to Gurtin [5] in his classic survey, tried to introduce the concept of elasticity in “a form palatable to both engineers and mathematicians”. However, such analytic methods are only suitable for problems with simple geometries, whereas with more general and complex geometries, numerical solutions must be employed.

One of the existing numerical approaches is the finite element method. Although the approach is general, actual implementation can become complicated when domain geometry with regions of different elastic properties are considered, e.g., composite systems with inclusions of different materials. If the geometric properties of the problem necessitate the use of multi-scale grids, spurious refraction or dispersion in wave propagation can arise at the boundaries separating grids of different length scales. In cases where an infinite domain is involved, one further needs to construct the effective outer boundary condition in order to satisfy the Sommerfeld radiation condition at infinity.

Another approach is the boundary element method (BEM) that involves the solution of surface integral equations [6, 7]. Although the resulting matrix system is dense, one only needs to deal with a surface mesh coinciding with the geometry of the domain boundaries thereby reducing a 3D problem to a 2D problem, see for example Rizzo et al. [8], or Beskos [2, 9]. This approach involves handling of at least weakly singular but integrable kernels in the integral equations [10], unless a recently developed desingularization method is employed [11].

The objective of this paper is to apply the Helmholtz decomposition to dynamic elasticity problems in the frequency domain using the desingularized boundary element method that provides high precision with fewer number of unknowns or degrees of freedom. The key idea is to use the Helmholtz decomposition of the dynamic elastic equation as described in Landau and Lifshitz [12] and work directly with the displacement vector field, \mathbf{u} which is decoupled into the sum of a transversal field, \mathbf{u}_T and a longitudinal field, \mathbf{u}_L . The solution can then be framed in terms of a set of scalar Helmholtz equations that are coupled by given boundary conditions. The divergence free condition on the transversal component and the

curl free condition on the longitudinal component can both be framed as Helmholtz scalar equations. Furthermore, these Helmholtz equations, all of the form

$$\nabla^2 f + k^2 f = 0, \quad (1)$$

with f a scalar function and k the constant wavenumber, can be solved with a recently developed BEM method that does not involve singular integrals [11].

In conventional BEM applied to Helmholtz equations, it is common practice for the surface to be represented by planar area elements and the unknown functions are taken to be constant within each of these elements. The singularity of the Green's function implies that integrals in which the integration point and the observation point lie in the same area element need to be treated with care. Although the presence of the diverging integrands is an accepted feature of the BEM, it does raise the philosophical question as why a mathematical formulation of physical problems that are well-behaved on boundaries needs to contain mathematical singularities.

In our non-singular version of the BEM [11], the singularities associated with the Green's function are removed analytically so that the surface integrals do not contain diverging integrands. The unknowns are taken to be values of functions at points or nodes that define quadratic surface elements on the boundary. For numerical evaluation of the surface integrals, the value of the integrand at any point within each area element is obtained by quadratic interpolation from the nodal values and such integrals can be evaluated accurately by quadrature. This approach increases the precision over conventional BEM by about 2 orders of magnitude with the same number of degrees of freedom [11, 13].

It is sometimes believed that the singular integrals are necessary to create a diagonal dominant matrix after discretizing the integral equations. In theory this is correct, provided that one can calculate the singular terms accurately enough. In practice, however, this almost always leads to considerable errors. For example, for a simple Laplace problem with linear elements, the terms on the diagonal are equal to the sum of the terms off-diagonal [13]. Any small error will destroy the critical diagonal dominance. Our non-singular implementation circumvents this difficulty and as a bonus allows us to use higher order elements combined with quadrature to evaluate all integrals. As an additional advantage, it is no longer necessary to calculate the solid angle that simplifies the implementation.

The theory concerning dynamic linear elasticity is introduced in Sect. 2. A rigid sphere executing harmonic oscillatory motion with a constant amplitude in an infinite linear elastic material will be chosen as a benchmark example. The analytical solution for this problem is given in Sect. 3. Since to the best of our knowledge, it has not been presented elsewhere in the literature, the derivation of this result is sketched in the Appendix. The concept of the desingularized boundary element method is presented in Sect. 4. Some results for the aforementioned vibrating rigid sphere are presented in Sect. 5 including plots of the displacement field in the 3D domain. Although a simple example has been used as a proof of concept, nevertheless it illustrates the underlying physics and theoretical intricacies. For example, it is found that in the limit of very low wave numbers, each of the decomposed longitudinal and transversal fields will develop a large term of equal magnitude but of opposite sign so that their sum reduces to the correct static solution. Consequently, the BEM framework should be used with caution in the low frequency limit and a discussion of this issue is given in Sect. 6. For moderate wave numbers these problems do not occur. We also present results for elastic wave pulses generated by an oscillating rigid bowl-shaped object that has both convex and concave surfaces that can produce focused elastic waves. Concluding remarks are given in Sect. 7.

2 Dynamic Linear Elastic Waves

2.1 The Navier Equation

In the time domain, the classical equation of motion without body forces is

$$\nabla \cdot \boldsymbol{\Sigma} = \rho \frac{\partial^2 \mathbf{U}}{\partial t^2}, \quad (2)$$

where the stress tensor, $\boldsymbol{\Sigma}$ and the displacement field, \mathbf{U} are functions of position and time, t and ρ is the material density. Assuming a harmonic time variation with angular frequency, ω for both the stress tensor, $\boldsymbol{\Sigma} = \boldsymbol{\sigma} e^{-i\omega t}$ and displacement vector, $\mathbf{U} = \mathbf{u} e^{-i\omega t}$ one obtains, in the frequency domain:

$$\nabla \cdot \boldsymbol{\sigma} = -\rho \omega^2 \mathbf{u}. \quad (3)$$

The infinitesimal strain tensor $\boldsymbol{\epsilon}$ is given in terms of the gradient of \mathbf{u} and its transpose:

$$\boldsymbol{\epsilon} = \frac{1}{2}(\nabla \mathbf{u} + [\nabla \mathbf{u}]^T). \quad (4)$$

For a linear elastic isotropic and homogeneous material, $\boldsymbol{\sigma}$ and $\boldsymbol{\epsilon}$ are related by Hooke's Law

$$\frac{\boldsymbol{\sigma}}{2\mu} = \left[\frac{c_L^2}{2c_T^2} - 1 \right] \text{tr}(\boldsymbol{\epsilon}) \mathbf{I} + \boldsymbol{\epsilon}, \quad (5)$$

with \mathbf{I} the identity tensor, the trace operator $\text{tr}(\boldsymbol{\epsilon}) \equiv \epsilon_{ii}$ (adopting the convention of summation over repeated indices of Cartesian tensors), the constants c_L and c_T are the longitudinal dilatational and transversal shear wave velocities, respectively, that are defined in terms of the Lamé constants λ and μ [12]:

$$c_L^2 = (\lambda + 2\mu)/\rho, \quad (6a)$$

$$c_T^2 = \mu/\rho. \quad (6b)$$

Introducing Eq. (5) into Eq. (3) we obtain two equivalent forms of the Navier equation

$$(c_L^2 - c_T^2)\nabla(\nabla \cdot \mathbf{u}) + c_T^2\nabla^2\mathbf{u} + \omega^2\mathbf{u} = \mathbf{0}, \quad (7a)$$

$$c_L^2\nabla(\nabla \cdot \mathbf{u}) - c_T^2\nabla \times \nabla \times \mathbf{u} + \omega^2\mathbf{u} = \mathbf{0}, \quad (7b)$$

where Eq. (7b) follows from the identity: $\nabla \times \nabla \times \mathbf{u} = \nabla(\nabla \cdot \mathbf{u}) - \nabla^2\mathbf{u}$. This result will be the starting point of our subsequent analysis. It will be shown that Eq. (7b) can be used for the analysis of dynamic linear elasticity by applying a Helmholtz decomposition to the displacement field. It turns out that the resulting equations can all be expressed in terms of scalar Helmholtz equations.

2.2 The Helmholtz Decomposition Applied to Dynamic Linear Elasticity

In this section a Helmholtz decomposition will be applied to the Navier equation (Eq. (7b)). It is well known [12] that the displacement vector \mathbf{u} can be decomposed into a transversal and a longitudinal part as

$$\mathbf{u} = \mathbf{u}_T + \mathbf{u}_L, \quad (8)$$

in which the transversal \mathbf{u}_T and the longitudinal \mathbf{u}_L displacements satisfy

$$\nabla \cdot \mathbf{u}_T = 0, \quad (9)$$

$$\nabla \times \mathbf{u}_L = \mathbf{0}. \quad (10)$$

We now define two wave numbers, one for the transversal component $k_T = \omega/c_T$ and one for the longitudinal component $k_L = \omega/c_L$ (noting that from Eqs. (6a), (6b), $k_T^2 > 2k_L^2$). Substituting Eq. (8) into Eq. (7b) and taking into account the conditions of Eqs. (9) and (10), it can easily be seen that both \mathbf{u}_T and \mathbf{u}_L satisfy the vector Helmholtz wave equation [12]:

$$\nabla^2 \mathbf{u}_T + k_T^2 \mathbf{u}_T = \mathbf{0}, \quad (11)$$

$$\nabla^2 \mathbf{u}_L + k_L^2 \mathbf{u}_L = \mathbf{0}. \quad (12)$$

These furnish six scalar Helmholtz equations, for each of the x , y and z component of the transversal and longitudinal displacements. However, the divergence and curl free conditions of Eq. (9) and Eq. (10) still need to be satisfied separately. It turns out that we can also cast these conditions as additional Helmholtz scalar equations.

2.3 Longitudinal Waves, \mathbf{u}_L

The zero curl condition, Eq. (10), of the longitudinal part of the displacement vector (also commonly referred to as compression wave), \mathbf{u}_L can be satisfied by introducing a scalar potential ϕ , where

$$\mathbf{u}_L \equiv \nabla \phi. \quad (13)$$

Equation (12) and Eq. (10) can then be replaced by the scalar Helmholtz equation:

$$\nabla^2 \phi + k_L^2 \phi = 0. \quad (14)$$

2.4 Transversal Waves, \mathbf{u}_T

The zero divergence condition, Eq. (9), of the transversal part of the displacement vector (a shear wave), \mathbf{u}_T can be satisfied by the following general vector identity

$$\nabla^2(\mathbf{x} \cdot \mathbf{u}_T) - \mathbf{x} \cdot \nabla^2 \mathbf{u}_T = 2\nabla \cdot \mathbf{u}_T, \quad (15)$$

with \mathbf{x} being the position vector: $\mathbf{x} = (x, y, z)$. Substituting Eqs. (9) and (11) into Eq. (15) gives

$$\nabla^2(\mathbf{x} \cdot \mathbf{u}_T) + k_T^2(\mathbf{x} \cdot \mathbf{u}_T) = 0. \quad (16)$$

This is just another Helmholtz equation for the scalar function $(\mathbf{x} \cdot \mathbf{u}_T)$. The origin of \mathbf{x} can be chosen arbitrarily as can be seen by taking the dot product of a constant vector, \mathbf{b} with Eq. (11) and subtracting this from Eq. (16), the result will be a similar equation as Eq. (16), but with the vector \mathbf{x} replaced by $(\mathbf{x} - \mathbf{b})$. Thus the transversal part can be described with four scalar Helmholtz equations: one for each of the 3 components of \mathbf{u}_T and one for $(\mathbf{x} \cdot \mathbf{u}_T)$.

Such an approach has been used successfully in electromagnetic scattering problems [14] where the electric field \mathbf{E} is divergence free: $\nabla \cdot \mathbf{E} = 0$ and satisfies the vector wave equation: $\nabla^2 \mathbf{E} + k^2 \mathbf{E} = \mathbf{0}$ (interested readers are referred to [15, 16]).

2.5 Solution Strategy

To summarize the above findings, the dynamic linear elastic problem can be expressed in terms of four Helmholtz equations with wavenumber k_T ; three for the x, y, z components of \mathbf{u}_T (Eq. (11)) and one for the scalar function $(\mathbf{x} \cdot \mathbf{u}_T)$ in Eq. (16); and another Helmholtz equation with wavenumber k_L for the longitudinal potential ϕ (Eq. (14)). In the current implementation, the Helmholtz equations are solved with a boundary element method, which relates a function on the surface to its normal derivative (see also Sect. 4). In order to retrieve the longitudinal displacement vector \mathbf{u}_L , the following formula can be employed

$$\mathbf{u}_L = \frac{\partial\phi}{\partial n}\mathbf{n} + \frac{\partial\phi}{\partial t_1}\mathbf{t}_1 + \frac{\partial\phi}{\partial t_2}\mathbf{t}_2, \tag{17}$$

in which $\partial/\partial n \equiv \mathbf{n} \cdot \nabla$ is the normal derivative, \mathbf{n} is the unit normal vector, $\partial/\partial t_1 \equiv \mathbf{t}_1 \cdot \nabla$ and $\partial/\partial t_2 \equiv \mathbf{t}_2 \cdot \nabla$ are the two tangential derivatives along the unit tangential vectors \mathbf{t}_1 and \mathbf{t}_2 on the surface.

Essentially, the above described approach is a combination of the soundwave scalar Helmholtz solution for longitudinal waves of Sect. 2.3 (see also [11]) and the transversal wave approach similar to the one used in electromagnetic scattering (for more details see [15] and [16]).

3 An Analytical Solution for a Vibrating Sphere

The analytical solution for a radially oscillating sphere as described in Lautrup [17] is well known but unfortunately it is less suitable as a numerical test case, since the transversal component is zero due to symmetry considerations.

Here we consider the waves generated in an elastic medium surrounding a rigid sphere with radius a , with the origin of the coordinate system located at the center of the sphere. The sphere executes harmonic displacement of constant amplitude so that in the frequency domain, the prescribed displacement on the surface of the sphere is $\mathbf{u} = \mathbf{u}_0$, with \mathbf{u}_0 a constant vector. The i th component ($i = x, y, z$) of the analytical solution for such a case is (see the Appendix for derivation)

$$\begin{aligned} u_i = & c_1 \left[e^{ik_T r} [1 + G(k_T r)] - e^{ik_L r} \frac{k_L^2}{k_T^2} G(k_L r) \right] \frac{2a}{r} u_i^0 \\ & + c_1 \left[e^{ik_T r} F(k_T r) - e^{ik_L r} \frac{k_L^2}{k_T^2} F(k_L r) \right] \frac{2a}{r^3} x_i (x_j u_j^0) \\ & - c_2 e^{ik_L r} [\delta_{ij} (ik_L r - 1) + x_i x_j k_L^2 F(k_L r)] \frac{a^3}{r^3} u_j^0, \end{aligned} \tag{18}$$

where r is the radial coordinate, δ_{ij} is the Kronecker delta function and the Einstein summation convention is taken over repeating indices. The functions $F(x)$ and $G(x)$ are defined as

$$F(x) = -1 - \frac{3i}{x} + \frac{3}{x^2}, \tag{19}$$

$$G(x) = \frac{i}{x} - \frac{1}{x^2}. \tag{20}$$

The terms proportional to $e^{ik_T r}$ correspond to the divergence free transversal part and the terms proportional to $e^{ik_L r}$ correspond to the curl free longitudinal part. The constants c_1 and c_2 can conveniently be expressed in terms of four other constants A, B, C and D as $c_1 = -B/(DA - BC)$ and $c_2 = A/(DA - BC)$ that are defined as:

$$A = 2e^{ik_T a} F(k_T a) - 2e^{ik_L a} (k_L/k_T)^2 F(k_L a), \tag{21a}$$

$$B = -e^{ik_L a} (k_L a)^2 F(k_L a), \tag{21b}$$

$$C = 2e^{ik_T a} [1 + G(k_T a)] - 2e^{ik_L a} (k_L/k_T)^2 G(k_L a), \tag{21c}$$

$$D = -e^{ik_L a} (ik_L a - 1). \tag{21d}$$

The method of constructing the solution in Eq. (18) is outlined in the Appendix. However, it can be verified by direct substitution that Eq. (18) is indeed a solution of the Navier equation with the boundary condition $u_i = u_i^0$ on the surface $r = a$ and it decays for large values of r .

Perhaps also worth mentioning, although we will not use it in the current work, is the solution that corresponds to the zero tangential stress boundary condition. That is, the boundary condition $u_i = u_i^0$ is replaced by $(\sigma_{ij} n_j) t_i = 0$ and $u_i n_i = u_i^0 n_i$ on the surface of the sphere. The constants A, C and D that appear in the coefficients c_1 and c_2 in Eq. (18) then have to be replaced by A', C' and D' (B remains the same) as

$$A' = e^{ik_T a} (ik_T a - 1) + A, \tag{22a}$$

$$C' = C + A, \tag{22b}$$

$$D' = D + B. \tag{22c}$$

4 Desingularized Boundary Element Method for Helmholtz Problems

In Sects. 2.2–2.4 it was shown that the problem of dynamic linear elasticity can be expressed in terms of five scalar Helmholtz equations in the form of Eq. (1): four of them with wavenumber k_T (Eqs. (11) and (16)) and another one with wavenumber k_L (Eq. (14)). Here it will be shown how a scalar Helmholtz equation can be solved efficiently using the framework of the boundary element method. The boundary element method has the advantage that only values of the unknown function on boundaries, S , need to be found, and from which values anywhere in the 3D domain can be calculated. In the context of Helmholtz equations, a further advantage of the boundary element method is the fact that the Sommerfeld radiation condition at infinity is automatically satisfied. Thus the boundary element method is especially suited for an object embedded in an infinite domain. Some recent advances in the boundary element method include the concept of full desingularization [18], which allows for high accuracy with reduced implementation effort.

The classical boundary element method is expressed as (see for example Becker [19], Kirkup [20] or any classical textbook on boundary element methods)

$$c(\mathbf{x}_0)\phi(\mathbf{x}_0) + \int_S \phi(\mathbf{x}) \frac{\partial H}{\partial n} dS(\mathbf{x}) = \int_S \frac{\partial \phi(\mathbf{x})}{\partial n} H dS(\mathbf{x}) \tag{23}$$

in which the Green’s function for the Helmholtz equation is defined as $H \equiv H(\mathbf{x}, \mathbf{x}_0) = e^{ikr}/r$, with k the wavenumber, $r = |\mathbf{x} - \mathbf{x}_0|$, and \mathbf{x}_0 and \mathbf{x} the observation and integration points, respectively. The variable $c(\mathbf{x}_0)$ is the solid angle when \mathbf{x}_0 is on the boundary

and $c = 4\pi$ when \mathbf{x}_0 is situated in the domain. The boundary element method relates the potential ϕ to its normal derivative $\partial\phi/\partial n$, where $\partial/\partial n \equiv \mathbf{n} \cdot \nabla$ (the unit normal vector on the surface S is $\mathbf{n} = \mathbf{n}(\mathbf{x})$ and points out of the domain). If, for example, ϕ (or $\partial\phi/\partial n$) is specified as a given boundary condition, then Eq. (23) can be solved for $\partial\phi/\partial n$ (or ϕ). If the surface S is discretized into N nodes, Eq. (23) can be written with respect to each node (corresponding to a different \mathbf{x}_0), and after the surface integrals are evaluated then results in a $N \times N$ linear matrix system to be solved numerically.

A relatively new concept, first introduced by Klaseboer et al. [13] is to replace $\phi(\mathbf{x})$ in Eq. (23) by a known analytical function $\chi(\mathbf{x})$ that also satisfies the Helmholtz equation, so that

$$c(\mathbf{x}_0)\chi(\mathbf{x}_0) + \int_S \chi(\mathbf{x}) \frac{\partial H}{\partial n} dS(\mathbf{x}) = \int_S \frac{\partial \chi(\mathbf{x})}{\partial n} H dS(\mathbf{x}). \tag{24}$$

In addition, $\chi(\mathbf{x})$ can be constructed to have the following properties:

$$\lim_{\mathbf{x} \rightarrow \mathbf{x}_0} \chi(\mathbf{x}) = \phi(\mathbf{x}_0), \tag{25}$$

$$\lim_{\mathbf{x} \rightarrow \mathbf{x}_0} \frac{\partial \chi(\mathbf{x})}{\partial n} = \frac{\partial \phi(\mathbf{x}_0)}{\partial n}, \tag{26}$$

so that when Eq. (24) is subtracted from Eq. (23), a fully desingularized boundary element method will emerge [11, 18]:

$$\int_S [\phi(\mathbf{x}) - \chi(\mathbf{x})] \frac{\partial H}{\partial n} dS(\mathbf{x}) = \int_S \left[\frac{\partial \phi(\mathbf{x})}{\partial n} - \frac{\partial \chi(\mathbf{x})}{\partial n} \right] H dS(\mathbf{x}). \tag{27}$$

Conveniently, the term with the solid angle $c(\mathbf{x}_0)$ no longer appears in Eq. (27). In this work, we can take

$$\chi(\mathbf{x}) = \phi(\mathbf{x}_0) \cos y + \frac{1}{k} \frac{\partial \phi(\mathbf{x}_0)}{\partial n} \sin y, \tag{28}$$

$$y = k \mathbf{n}(\mathbf{x}_0) \cdot (\mathbf{x} - \mathbf{x}_0), \tag{29}$$

so that Eq. (27) can then be written in full as:

$$\begin{aligned} & 4\pi\phi(\mathbf{x}_0) + \int_S \left\{ \phi(\mathbf{x}) - \phi(\mathbf{x}_0) \cos y + \frac{1}{k} \frac{\partial \phi(\mathbf{x}_0)}{\partial n} \sin y \right\} \frac{\partial H}{\partial n} dS(\mathbf{x}) \\ & = \int_S \left\{ \frac{\partial \phi(\mathbf{x})}{\partial n} - \frac{\partial \phi(\mathbf{x}_0)}{\partial n} [\mathbf{n}(\mathbf{x}_0) \cdot \mathbf{n}(\mathbf{x})] \cos y + k [\mathbf{n}(\mathbf{x}_0) \cdot \mathbf{n}(\mathbf{x})] \phi(\mathbf{x}_0) \sin y \right\} H dS(\mathbf{x}). \end{aligned} \tag{30}$$

Note that the terms with $\cos y$ perform the actual desingularization since y tends towards zero as \mathbf{x} approaches \mathbf{x}_0 , which cancels out the $1/r$ singularity caused by the Green’s function H and its normal derivative. Also $\mathbf{n}(\mathbf{x}_0) \cdot \mathbf{n}(\mathbf{x})$ tends towards unity when \mathbf{x} approaches \mathbf{x}_0 . In Eq. (30) the terms with $\phi(\mathbf{x}_0)$ and $\partial\phi(\mathbf{x}_0)/\partial n$ will end up on the diagonal of a resulting matrix system after a discretisation and numerical Gaussian integration has been performed. The term with $4\pi\phi(\mathbf{x}_0)$ originates from the fact that the choice of Eq. (28) when put into Eq. (24) will cause a contribution from the surface at infinity, which turns out to be exactly $4\pi\phi(\mathbf{x}_0)$. This term is only present for external problems (such as the ones described in the current work) and should be omitted for internal problems.

This framework is free of any weak, strong or hyper singularities associated with the usual implementation of the boundary element method in dynamic linear elasticity. Simple Gauss quadratures can therefore be employed to evaluate integrals over each element including the previously singular ones. In the current implementation, integration over quadratic six noded triangular elements was used with quadratic shape functions [15].

The normal derivative of $(\mathbf{x} \cdot \mathbf{u}_T)$ can be expressed in terms of the normal component of \mathbf{u}_T and the dot product of \mathbf{x} with the normal derivative of \mathbf{u}_T as:

$$\begin{aligned} \frac{\partial(\mathbf{x} \cdot \mathbf{u}_T)}{\partial n} &= \mathbf{u}_T \cdot \mathbf{n} + \mathbf{x} \cdot \frac{\partial \mathbf{u}_T}{\partial n} \\ &= u_{Tx}n_x + u_{Ty}n_y + u_{Tz}n_z + x \frac{\partial u_{Tx}}{\partial n} + y \frac{\partial u_{Ty}}{\partial n} + z \frac{\partial u_{Tz}}{\partial n}. \end{aligned} \tag{31}$$

The tangential derivatives in Eq. (17) were calculated using the average of the tangential derivatives on each neighboring element of a node. In the current implementation we used an iterative method with an LU-decomposition framework, such that effectively only two $N \times N$ matrix systems need to be solved (one for k_T and one for k_L). To start the iterative process, an estimation for the normal component of the transversal displacement is $u_{Tn}^m = \mathbf{u}_T \cdot \mathbf{n}$ is assumed (for the first iteration, $m = 1$ and $u_{Tn}^1 = 0$). Then, for the next iteration, the normal derivative of the potential is calculated as

$$\frac{\partial \phi^{m+1}}{\partial n} = (1 - \alpha) \frac{\partial \phi^m}{\partial n} + \alpha [\mathbf{u}_0 \cdot \mathbf{n} - u_{Tn}^m], \tag{32}$$

where a relaxation factor α was used. With the boundary element method (for k_L) an estimation for ϕ^{m+1} can now be found. Its tangential derivatives in the \mathbf{t}_1 and \mathbf{t}_2 direction can be calculated and \mathbf{u}_L^{m+1} is given by Eq. (17). Since on the boundary $\mathbf{u}_T = \mathbf{u}_0 - \mathbf{u}_L$, with $\mathbf{u}_0 = (U, 0, 0)$ prescribed, the transversal vector \mathbf{u}_T^{m+1} can be obtained. \mathbf{u}_T^{m+1} is then decomposed into its x , y and z components, and, for each component, we apply the boundary element method (now for k_T) to get $\partial u_{Tx}^{m+1} / \partial n$, $\partial u_{Ty}^{m+1} / \partial n$ and $\partial u_{Tz}^{m+1} / \partial n$. To satisfy the last Helmholtz equation corresponding to Eq. (16), the scalar $\mathbf{x} \cdot \mathbf{u}_T^{m+1}$ is given and its normal derivative is calculated with the boundary element method (again for k_T). Since $\partial u_{Tx}^{m+1} / \partial n$, $\partial u_{Ty}^{m+1} / \partial n$ and $\partial u_{Tz}^{m+1} / \partial n$ are already known, with the help of Eq. (31), a new estimate for u_{Tn}^{m+1} can be obtained. Then the iterative loop can be repeated until convergence is obtained. There are alternative approaches to solve the system of equations, some discussion on such solutions will be presented in Sect. 5.

5 Results

Results will now be shown for the vibrating sphere with $\mathbf{u}^0 = (U, 0, 0)$ and numerical BEM results are compared to the analytic solution of Sect. 3. In all examples, the sphere is represented by a mesh with 180 quadratic elements and $N = 362$ nodes. The field values were obtained through post-processing on a 40×40 grid covering an area of $10a \times 10a$ of the 3D domain outside the sphere. In Fig. 1, we compare analytic and numerical results for \mathbf{u}_L and \mathbf{u}_T with $k_L a = 2.0$, $k_T a = 1.0$. For this particular parameter set, \mathbf{u}_T is the dominant term. The agreement between theory and numerical results is excellent. This can be seen clearly in Fig. 2 where the average difference between the numerical solution and the analytic solution is less than 0.13%. Another set of comparisons with $k_T a = 4.0$ and $k_L a = 2.0$ is shown in Fig. 3 for which the \mathbf{u}_L component is slightly more prominent. In Fig. 4, the total field \mathbf{u} is

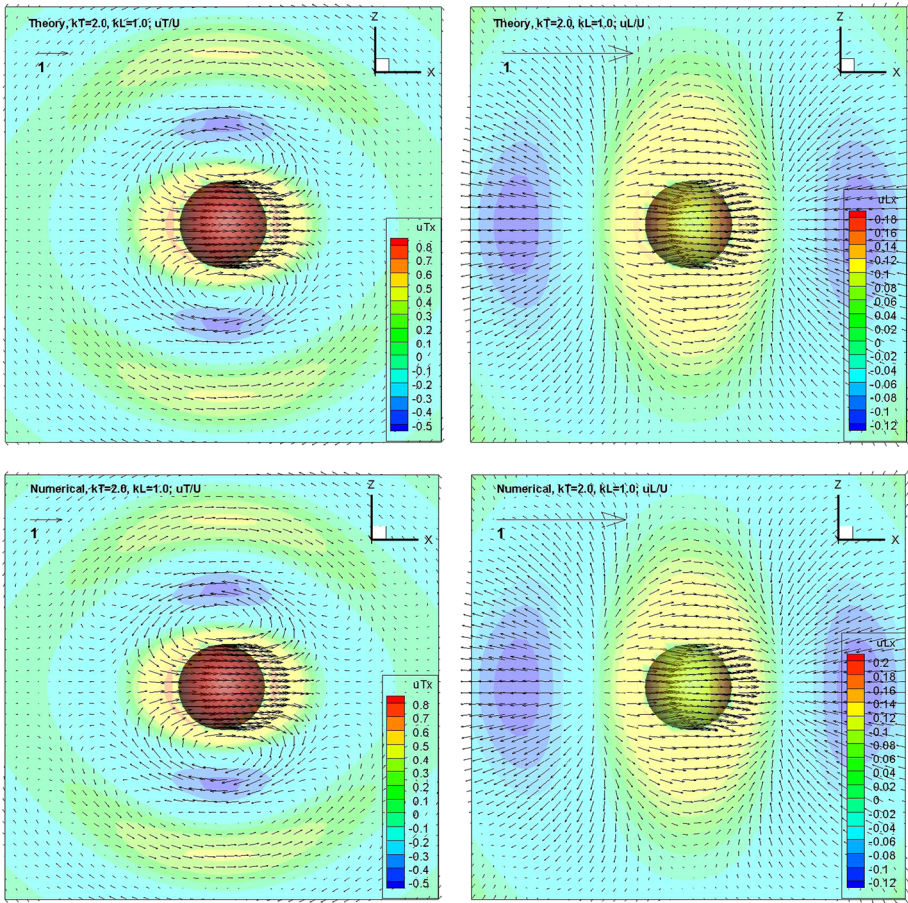


Fig. 1 Sphere with radius a vibrating in the x -direction defined by the boundary condition: $\mathbf{u}^0 = (U, 0, 0)$ on the sphere surface $r = a$ at $k_T a = 2.0$ and $k_L a = 1.0$. Surface and field plot of the displacement field vector \mathbf{u} scaled by U . Analytical results for \mathbf{u}_T and \mathbf{u}_L are given in the top left and right images and corresponding numerical BEM results are shown in the lower images. For this particular case \mathbf{u}_T is the dominant term. For corresponding BEM movies to these figures see Sect. 8

shown for both parameter sets. In Fig. 5, the total field \mathbf{u} for a bowl-shaped oscillator with convex and concave surfaces vibrating parallel and perpendicular to its axis of symmetry is shown. The shape of this axisymmetric bowl-shaped oscillator is obtained by rotating the following curve around the x -axis (see Eq. (6) in [21] and also [22] for an application in acoustic waves)

$$(x/a, z/a) = (\beta \sin^2 \alpha + \gamma [\cos \alpha - 1], 2 \sin \alpha), \quad 0 \leq \alpha \leq 2\pi, \tag{33}$$

where the parameters $\beta = 0.6$, $\gamma = 0.5$, $k_T a = 5$ and $k_L a = 2$ are chosen in Fig. 5.

Once the (complex) displacements fields: \mathbf{u} , \mathbf{u}_T or \mathbf{u}_L are obtained, we can make use of the fact that when this solution is multiplied by a constant phase factor, i.e. $\mathbf{u} \exp(i\alpha)$, it is also a solution of the system. This was used to reconstruct the solution in the time domain and get the solution at different time intervals. The movie files thus created are available as supplementary material. For a list of movie files see Sect. 8.

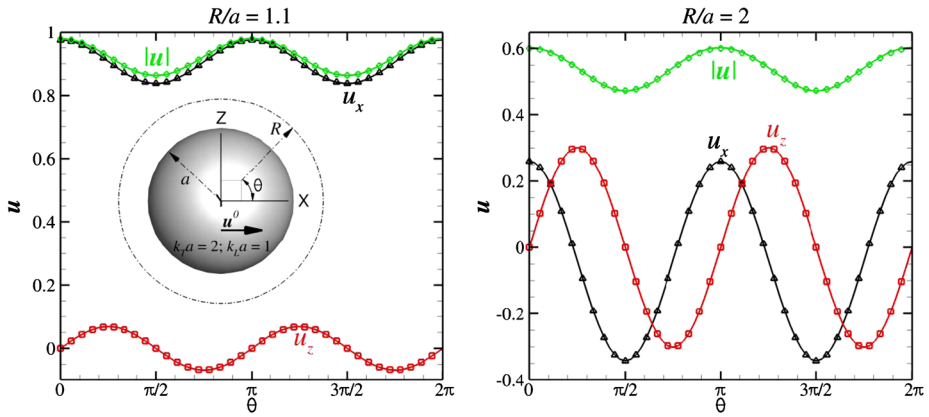


Fig. 2 Same as in Fig. 1, field displacement \mathbf{u} scaled by U along circles with radii (left) $R/a = 1.1$ and (right) $R/a = 2$ on plane $y = 0$. Lines: analytic solutions; symbols: numerical solutions

In addition to the iterative solution framework discussed in Sect. 4, a direct solution using a bigger matrix system was also investigated. One option is to solve directly for the 5 unknowns $\phi, \partial\phi/\partial n, \partial u_{Tx}/\partial n, \partial u_{Ty}/\partial n$ and $\partial u_{Tz}/\partial n$ resulting in a matrix system which is $5N \times 5N$ in size (where N is the number of nodes), here we still solve five Helmholtz equations, but now do so simultaneously without iteration. Another option is not to work with the potential representation for $\mathbf{u}_L = \nabla\phi$, but work directly with the \mathbf{u}_L vector and its normal derivatives, this will result in a system of $9N \times 9N$ equations. Here, we do not recommend the above mentioned approaches for the following reasons: firstly, the matrix system is very large, resulting in rather long computational times. Secondly, the condition number of the $5N$ and $9N$ systems appears to be quite large resulting in spurious solutions for the decomposed vectors (nevertheless, the field vectors of the total displacement field appear to remain very accurate).

The advantage of the current iterative method over a full tensor description like the one used by Rizzo et al. [8] is that our method uses $N \times N$ matrices, while they use $3N \times 3N$ matrices (since there are three components for the displacement and traction in 3D). The current approach is also conceptually simpler than that of Rizzo et al. [8], since there are no singular integrals to be considered. Moreover, with their method, one cannot get the transversal and longitudinal components which might have important physical implications since they travel at different speeds c_L and c_T as given by Eq. (6). This is apparent in earthquake science with the clear distinction between arrival times of P waves and S waves.

6 Discussion: The Zero Frequency Divergence

One final issue worth mentioning is the appearance of a zero frequency divergence of the decomposed displacement vectors \mathbf{u}_L and \mathbf{u}_T . Equation (18) can alternatively be written as:

$$u_i = c_1 a U_{ij} u_j^0 - c_2 a^3 \frac{\partial^2}{\partial x_i \partial x_j} \frac{e^{ik_L r}}{r} u_j^0. \tag{34}$$

The term with c_1 is actually proportional to the Green's function of the dynamic linear elastic problem U_{ij} , and the term proportional to c_2 is a dipole tensor. Let us investigate the analytical solution when the frequency ω goes to zero. By doing a Taylor expansion of e^{ix} to

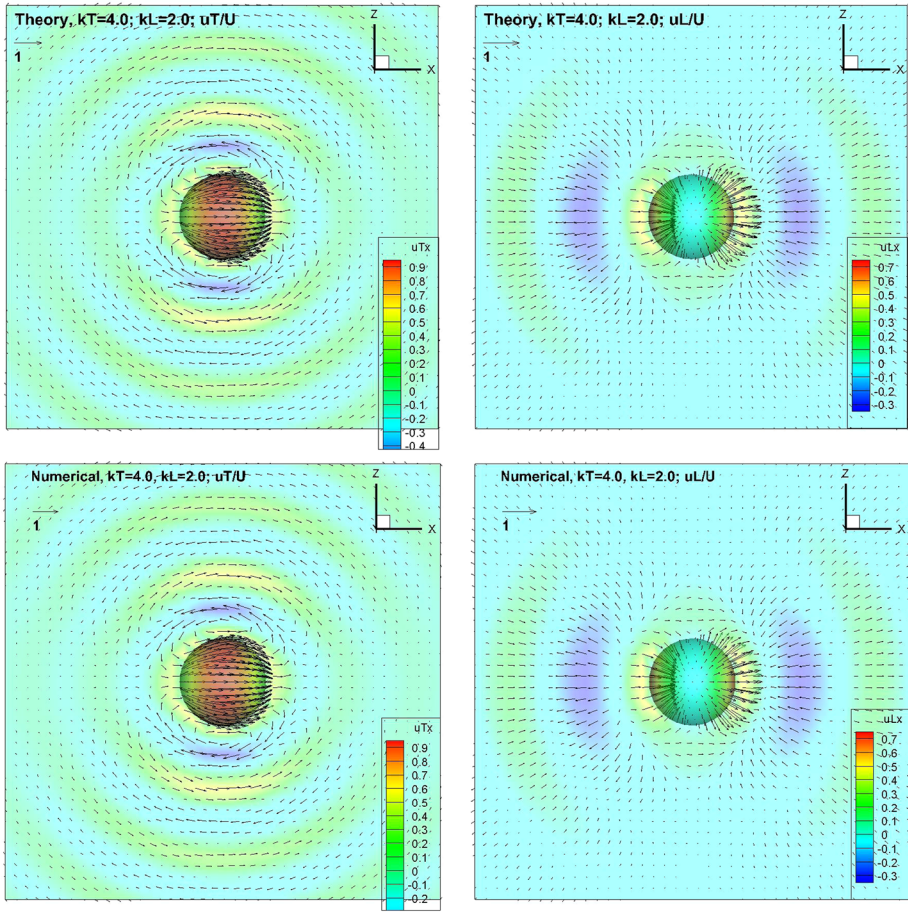


Fig. 3 As for Fig. 1 but with parameters $k_T a = 4.0$ and $k_L a = 2.0$. The u_T and u_L vectors are now comparable in magnitude. For corresponding movies see Sect. 8

the second order i.e. $e^{ix} = 1 + ix - x^2/2 + o(x^3)$, where x is either $k_T r$ or $k_L r$, in the limit of the zero frequency, $k_L \rightarrow 0$, $k_T \rightarrow 0$, and the terms in Eq. (18) can be approximated by

$$\lim_{k_L, k_T \rightarrow 0} e^{ix} [1 + G(x)] = -\frac{1}{x^2} + \frac{1}{2}, \tag{35}$$

$$\lim_{k_L, k_T \rightarrow 0} e^{ix} G(x) = -\frac{1}{x^2} - \frac{1}{2}, \tag{36}$$

$$\lim_{k_L, k_T \rightarrow 0} e^{ix} F(x) = \frac{3}{x^2} + \frac{1}{2}. \tag{37}$$

The first term with c_1 in Eq. (18) can now be approximated with

$$\begin{aligned} & \lim_{k_L, k_T \rightarrow 0} \left\{ e^{ik_T r} [1 + G(k_T r)] - \frac{k_L^2}{k_T^2} e^{ik_L r} G(k_L r) \right\} \\ &= -\frac{1}{k_T^2 r^2} + \frac{1}{2} - \frac{k_L^2}{k_T^2} \left[-\frac{1}{k_L^2 r^2} - \frac{1}{2} \right] = \frac{1}{2} \left[1 + \frac{k_L^2}{k_T^2} \right]. \end{aligned} \tag{38}$$

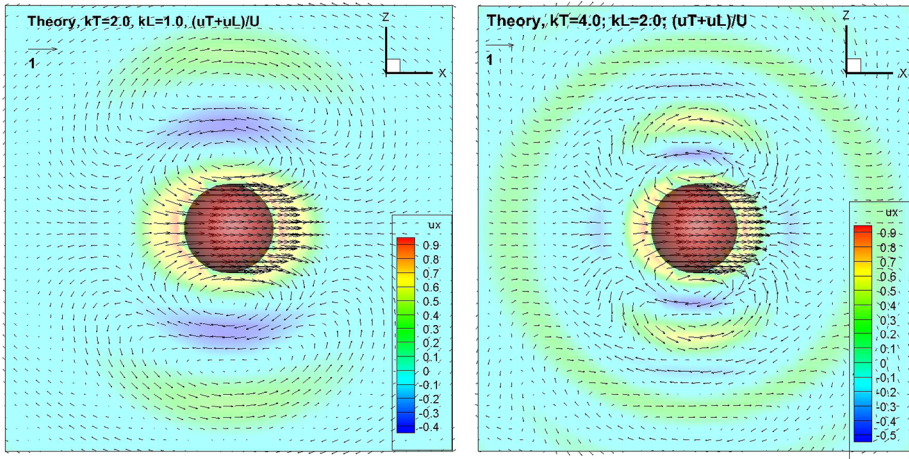


Fig. 4 Sphere vibrating in the x -direction, surface and field plot of the total theoretical $\mathbf{u} = \mathbf{u}_T + \mathbf{u}_L$ vector field; left $k_T a = 2.0$ and $k_L a = 1.0$; right $k_T a = 4.0$ and $k_L a = 2.0$. The numerical fields are virtually indistinguishable from those above (not shown). For corresponding movies see Sect. 8

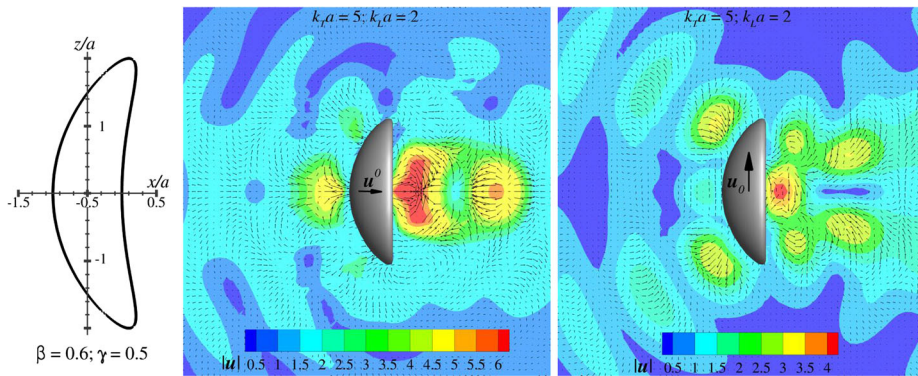


Fig. 5 Bowl-shaped oscillator (left) vibrating in (middle) the x -direction parallel to its axis of symmetry and (right) z -direction perpendicular to its axis of symmetry, field plot of \mathbf{u} vector field scaled by U obtained numerically; $k_T a = 5.0$ and $k_L a = 2.0$. The wave focusing effect of the bowl-shaped object can clearly be observed, even in the case of the oscillation in the z -direction, perpendicular to the axis of symmetry of the bowl (right). For corresponding movies see Sect. 8

It can be seen that the transversal (with $e^{ik_T r}$) and the longitudinal (with $e^{ik_L r}$) terms both diverge with $1/k_T^2$, but the singularities cancel each other out when they are summed. Similarly, the second term with c_1 in Eq. (18) now becomes

$$\begin{aligned} & \lim_{k_L, k_T \rightarrow 0} \left\{ e^{ik_T r} F(k_T r) - \frac{k_L^2}{k_T^2} e^{ik_L r} F(k_L r) \right\} \\ &= \frac{3}{k_T^2 r^2} + \frac{1}{2} - \frac{k_L^2}{k_T^2} \left[\frac{3}{k_L^2 r^2} + \frac{1}{2} \right] = \frac{1}{2} \left[1 - \frac{k_L^2}{k_T^2} \right]. \end{aligned} \tag{39}$$

Again, the transversal and longitudinal terms both diverge with $1/k_T^2$ but cancel each other out. The term in Eq. (18) proportional to c_2 does not diverge. The constants c_1 and c_2 can also be expressed in the zero frequency limit as:

$$c_1^0 = \lim_{k_L, k_T \rightarrow 0} c_1 = \lim_{k_L, k_T \rightarrow 0} \frac{-B}{DA - BC} = \frac{3}{4 + 2k_L^2/k_T^2}, \tag{40}$$

$$c_2^0 = \lim_{k_L, k_T \rightarrow 0} c_2 = \lim_{k_L, k_T \rightarrow 0} \frac{A}{DA - BC} = \frac{1 - k_L^2/k_T^2}{4 + 2k_L^2/k_T^2}. \tag{41}$$

Thus in the limit of $k_L, k_T \rightarrow 0$, the displacement field becomes

$$u_i = ac_1^0 \left[\frac{u_i^0}{r} + \frac{x_i x_j u_j^0}{r^3} + \frac{k_L^2}{k_T^2} \left(\frac{u_i^0}{r} - \frac{x_i x_j u_j^0}{r^3} \right) \right] + a^3 c_2^0 \left[\frac{u_i^0}{r^3} - \frac{3x_i x_j u_j^0}{r^5} \right]. \tag{42}$$

In Eq. (42), the first two terms, $u_i^0/r + x_i x_j u_j^0/r^3$, represent a so-called Stokeslet that is a divergence free part of the solution. The terms with k_L^2/k_T^2 in front represent the curl free part. The last part that is proportional to c_2^0 is both divergence and curl free, which makes the Helmholtz decomposition non-unique in the zero frequency case. Both Eqs. (11) and (12) then revert back to the Laplacian. Even though k_L and k_T are both zero, their ratio in Eq. (42) remains finite since from Eq. (6) one can obtain

$$\frac{k_L^2}{k_T^2} = \frac{c_T^2}{c_L^2} = \frac{\mu}{\lambda + 2\mu}. \tag{43}$$

The fact that the transversal and longitudinal part of Eqs. (38) and (39) diverge when the frequency approaches zero poses some limitations on the proposed boundary element framework where we separated the solution into a divergence and a curl free part. Note that the Rizzo [8] solution does not diverge in this limit since it does not use the Helmholtz decomposition to split \mathbf{u} into \mathbf{u}_T and \mathbf{u}_L but works with the total displacement \mathbf{u} and the traction instead, however, strong singularities will show up in their method at zero frequency. Since the divergence occurs in the Green’s function U_{ij} , it is highly likely that any $\mathbf{u}_T, \mathbf{u}_L$ decomposition for an arbitrary object will exhibit the same singular behavior.

Note that this divergence is unrelated to the zero frequency catastrophe encountered in certain numerical implementations of electromagnetic scattering (see for example Chew [23]), since it originates there from the decoupling of the electric and magnetic field at zero frequency, whereas in the current case the cause of the divergence is the Helmholtz decomposition of the displacement field.

7 Conclusion

The dynamic linear elasticity problem was tackled by working with the displacement field, \mathbf{u} , using a Helmholtz decomposition. The transversal, \mathbf{u}_T and longitudinal, \mathbf{u}_L components were all solved with desingularized Helmholtz boundary element methods, with one scalar Helmholtz equation for the scalar potential, ϕ of the longitudinal part and three scalar Helmholtz equations for the three Cartesian components of the transversal part plus an additional scalar Helmholtz equation to enforce the divergence free condition of \mathbf{u}_T . To minimize the need to solve large matrix equations, this systems of 5 scalar Helmholtz equations are solved by an iterative method.

It was shown that this numerical approach is viable by comparing the results to that of an analytical solution for a vibrating sphere for two different sets of parameters with ka around unity. Theoretically it was shown that the framework will fail for very low ka numbers, since the transversal and longitudinal part both diverge. However, the total displacement remains well-behaved and finite. Thus the current framework works best for moderately high ka numbers.

8 Complementary Material Description

The following movies are available as complementary material and correspond to the test cases described in the text:

1. **01m_Theory_uTotal_kT2_kL1b.mp4** shows the total displacement field \mathbf{u} for the parameters $k_T a = 2.0$ and $k_L a = 1.0$. At several radii away from the sphere, the main displacement occurs around the z -axis in the horizontal direction. The contour plots correspond to the x -component of the \mathbf{u} vector.
2. **02m_Theory_uTotal_kT2_kL1b.mp4** as the previous movie, but now the contour plots are for the z -component of the \mathbf{u} vector.
3. **03m_Theory_uT_kT2_kL1b.mp4** the same parameters as for the previous movies, but now the transversal components \mathbf{u}_T are shown. The main transversal waves move away from the sphere along the z -axis. The x -component is shown as a contour plot.
4. **04m_Theory_uL_kT2_kL1b.mp4** the same parameters as for the previous movies, but now the longitudinal components \mathbf{u}_L are shown (with the x -component again as a contour plot). The main longitudinal waves are moving along the x -axis.
5. **05m_Theory_uTotal_kT4_kL2b.mp4** shows the total displacement field \mathbf{u} for the parameters $k_T a = 4.0$ and $k_L a = 2.0$. Due to these higher ka numbers the wavelengths are shorter. The contour plots are for the x -component. The overall pattern at some distance away from the sphere appears to be more ‘radial’ in nature than for the parameters $k_T a = 2.0$ and $k_L a = 1.0$.
6. **06m_Theory_uTotal_kT4_kL2b.mp4** is the same as the previous movie, but now with the contour plot for the z -component.
7. **07m_Theory_uT_kT4_kL2b.mp4** as for the previous two movies, but now the transversal decomposed vector field \mathbf{u}_T is shown. It appears to ‘radiate’ mainly in the z -direction.
8. **08m_Theory_uL_kT4_kL2b.mp4** as for the previous three movies, now for the longitudinal decomposed vector field \mathbf{u}_L . This time the waves ‘radiate’ outwards mainly in the x -direction.
9. **09m_Bowl_u_kT5_kL2_parallel.mp4** shows the total displacement field \mathbf{u} for the parameters $k_T a = 5.0$ and $k_L a = 2.0$ when a bowl-shaped oscillator vibrates along its axis of symmetry. The contour plots correspond to the magnitude of the \mathbf{u} vector.
10. **10m_Bowl_u_kT5_kL2_perpendicular.mp4** shows the total displacement field \mathbf{u} for the parameters $k_T a = 5.0$ and $k_L a = 2.0$ when a bowl-shaped oscillator vibrates perpendicular to its axis of symmetry. The contour plots correspond to the magnitude of the \mathbf{u} vector.

The movie files are best appreciated when the player is put in the “loop” mode. The vectors on the surface of the sphere have been suppressed in the plotting routine in order to see the vectors in the field better.

Appendix: An Oscillating Rigid Sphere in an Elastic Medium

In this Appendix, we sketch the derivation of the analytic solution that describes the periodic movement of a rigid no-slip sphere of radius, a in an infinite elastic medium. This solution is inspired by the well-known analytic solution of a similar sphere in a quiescent viscous liquid at low Reynolds number or Stokes flow with the following governing equations for the velocity \mathbf{u} and pressure p : $\mu \nabla^2 \mathbf{u} = \nabla p$ and $\nabla \cdot \mathbf{u} = 0$, with μ the viscosity of the liquid. The solution for the velocity field, in tensor notation, is:

$$u_i^{Stokes} = \left[\frac{3a}{4r} + \frac{a^3}{4r^3} \right] u_i^0 + \frac{3}{4a^2} \left[\frac{a^3}{r^3} - \frac{a^5}{r^5} \right] x_i (x_j u_j^0), \tag{44}$$

with u_i^0 being the velocity of the sphere, that is, $\mathbf{u} = \mathbf{u}^0$ on the sphere surface and \mathbf{u} decays as $1/r$ towards infinity. Integration of the corresponding traction over the surface of the sphere leads to the Stokes formula for the drag force on a sphere: $\mathbf{F}_d = (6\pi \mu a) \mathbf{u}^0$.

Equation (44) can be rewritten in a more convenient form for our analysis as:

$$u_i^{Stokes} = \left(\frac{3a}{4} \right) \left[\frac{\delta_{ij}}{r} + \frac{x_i x_j}{r^3} \right] u_j^0 + \left(\frac{a^3}{4} \right) \left[\frac{\delta_{ij}}{r^3} - 3 \frac{x_i x_j}{r^5} \right] u_j^0 \tag{45a}$$

$$\equiv \left(\frac{3a}{4} \right) G_{ij}^{Stokes} u_j^0 - \left(\frac{a^3}{4} \right) \nabla \left(\nabla \frac{1}{r} \right) \cdot \mathbf{u}_0. \tag{45b}$$

The term: $G_{ij}^{Stokes} \equiv \left[\frac{\delta_{ij}}{r} + \frac{x_i x_j}{r^3} \right]$ is a Stokeslet or the Green’s function for Stokes flow whereas the second term: $\frac{\partial^2}{\partial x_i \partial x_j} \left(\frac{1}{r} \right) = \nabla \left(\nabla \frac{1}{r} \right)$ is the dipolar Green’s function of the Laplace equation: $\nabla^2 \phi = 0$.

Now we observe that the dipolar term: $\nabla \left(\nabla \frac{1}{r} \right)$ is a solution of the governing equation for static linear elasticity:

$$\left[\frac{k_T^2}{k_L^2} - 1 \right] \nabla \nabla \cdot \mathbf{u} + \nabla^2 \mathbf{u} = 0, \tag{46}$$

so analogous to Eqs. (45a), (45b) we seek a general solution of Eq. (46) of the form

$$u_i^{LE} = c_1 a G_{ij}^{LE} u_j^0 - c_2 a^3 \left(\frac{\partial^2}{\partial x_i \partial x_j} \frac{1}{r} \right) u_j^0, \tag{47}$$

where c_1 and c_2 are constants to be determined and G_{ij}^{LE} is the Green’s for the static linear elastic equation

$$G_{ij}^{LE} \equiv \left[\frac{\delta_{ij}}{r} + \frac{x_i x_j}{r^3} \right] + \frac{k_L^2}{k_T^2} \left[\frac{\delta_{ij}}{r} - \frac{x_i x_j}{r^3} \right]. \tag{48}$$

We find the constants c_1 and c_2 using the boundary condition at $r = a$: $u_i^{LE} = u_i^0$ which leads to

$$u_i^{LE} = u_i^0 = u_i^0 \left[\left\{ 1 + \frac{k_L^2}{k_T^2} \right\} c_1 + c_2 \right] + \frac{x_i x_j}{a^2} u_j^0 \left[\left\{ 1 - \frac{k_L^2}{k_T^2} \right\} c_1 - 3c_2 \right] \text{ at } r = a. \tag{49}$$

The second term in square brackets must be zero and the first term in square brackets must then be equal to 1. Thus solving for c_1 and c_2 results in:

$$c_1 = \frac{3k_T^2}{4k_T^2 + 2k_L^2}, \quad (50)$$

$$c_2 = \frac{k_T^2 - k_L^2}{4k_T^2 + 2k_L^2}. \quad (51)$$

This approach can be extended to the *dynamic* linear elastic case by taking a linear combination of the Green's function for dynamic linear elasticity and a term proportional to the Helmholtz dipole $\frac{\partial^2}{\partial x_i \partial x_j} \left(\frac{\exp(ikr)}{r} \right) u_j^0$. For dynamic linear elasticity, the vector \mathbf{u} represents the velocity amplitude of a vibrating sphere that is a constant in the frequency domain. After some algebra, this approach leads eventually to Eq. (18).

References

1. Iturrarán-Viveros, U., Sánchez-Sesma, F.J., Luzón, F.: Boundary element simulation of scattering of elastic waves by 3-D cracks. *J. Appl. Geophys.* **64**, 70–82 (2008)
2. Beskos, D.E.: Boundary element methods in dynamic analysis. *Appl. Mech. Rev.* **40**, 1–23 (1987)
3. Dual, J., Schwarz, T.: Acoustofluidics 3: continuum mechanics for ultrasonic particle manipulation. *Lab Chip* **12**, 244–252 (2012)
4. Sternberg, E.: On the integration of the equations of motion in the classical theory of elasticity. *Arch. Ration. Mech. Anal.* **6**, 34–50 (1960)
5. Gurtin, M.E.: *The Linear Theory of Elasticity*. Springer, Berlin (1973)
6. Cruse, T.A., Rizzo, F.J.: A direct formulation and numerical solution of the general transient elastodynamic problem. *I. J. Math. Anal. Appl.* **22**, 244–259 (1968)
7. Cruse, T.A.: A direct formulation and numerical solution of the general transient elastodynamic problem. *II. J. Math. Anal. Appl.* **22**, 341–355 (1968)
8. Rizzo, F.J., Shippy, D.J., Rezayat, M.: A boundary integral equation method for radiation and scattering of elastic waves in three dimensions. *Int. J. Numer. Methods Eng.* **21**, 115–129 (1985)
9. Beskos, D.E.: Boundary element methods in dynamic analysis: part II (1986–1996). *Appl. Mech. Rev.* **50**, 149–197 (1997)
10. Bu, F., Lin, J., Reitich, F.: A fast and high-order method for the three-dimensional elastic wave scattering problem. *J. Comput. Phys.* **258**, 856–870 (2014)
11. Sun, Q., Klaseboer, E., Khoo, B.C., Chan, D.Y.C.: Boundary regularized integral equation formulation of the Helmholtz equation in acoustics. *R. Soc. Open Sci.* **2**, 140520 (2015)
12. Landau, L.D., Lifshitz, E.M.: *Theory of Elasticity*. Pergamon Press Ltd., Oxford (1959)
13. Klaseboer, E., Rosalez-Fernandez, C., Khoo, B.C.: A note on true desingularization of boundary element methods for three-dimensional potential problems. *Eng. Anal. Bound. Elem.* **33**, 796–801 (2009)
14. Harrington, R.F.: *Time-Harmonic Electromagnetic Fields* p. 38. John Wiley & Sons, Inc., New York (2001)
15. Klaseboer, E., Sun, Q., Chan, D.Y.C.: Nonsingular field-only surface integral equations for electromagnetic scattering. *IEEE Trans. Antennas Propag.* **65**, 972–977 (2017)
16. Sun, Q., Klaseboer, E., Chan, D.Y.C.: Robust multiscale field-only formulation of electromagnetic scattering. *Phys. Rev. B* **95**, 045137 (2017)
17. Lautrup, B.: *Physics of Continuous Matter*, vol. 12, 2nd edn. p. 204. CRC Press/Taylor and Francis, Boca Raton (2011). Section 12.6
18. Klaseboer, E., Sun, Q., Chan, D.Y.C.: Non-singular boundary integral methods for fluid mechanics applications. *J. Fluid Mech.* **696**, 468–478 (2012)
19. Becker, A.A.: *The Boundary Element Method in Engineering: A Complete Course*. McGraw-Hill International (UK) Limited, London (1992)
20. Kirkup, S.: *The Boundary Element Method in Acoustics* (1998). ISBN 0-953-4031-06
21. Klaseboer, E., Sun, Q., Chan, D.Y.C.: Field-only integral equation method for time domain scattering of electromagnetic pulses. *Appl. Opt.* **56**, 9377–9383 (2017)

22. Klaseboer, E., Sepehrirahnama, S., Chan, D.Y.C., Klaseboer, E.: Space-time domain solutions of the wave equation by a non-singular boundary integral method and Fourier transform. *J. Acoust. Soc. Am.* **142**, 697–707 (2017)
23. Chew, W.C., Tong, M.S., Hu, B.: *Integral Equation Methods for Electromagnetic and Elastic Waves*. Morgan & Claypool, San Rafael (2009)